

Structural, elastic, mechanical and optoelectronic properties of zinc-doped SrTiO₃ perovskite compounds

F. Benlakhda*, M. A. Ghebouli*, Z. Zerrougui[†], K. Bouferrache[‡],
Y. Slimani[§], B. Ghebouli[¶], I. Bouchama*^{||}, T. Chih^{*}, M. Fatmi^{*,††},
Saif A. Mouhammad^{**}, Norah Algethami^{**} and Sultan Alomairy^{**}

*Research Unit on Emerging Materials (RUEM), University Ferhat Abbas of Setif 1,
Setif 19000, Algeria

[†]Laboratory of Studies Surfaces and Interfaces of Solids Materials,
Faculty of Technology, University Ferhat Abbas of Setif 1,
Setif 19000, Algeria

[‡]Department of Physics, Faculty of Sciences,
University of Mohamed Boudiaf, M'sila 28000, Algeria

[§]Laboratory of Intelligent System (LSI), Faculty of Technology,
University Ferhat Abbas of Setif 1, Setif 19000, Algeria

[¶]Laboratory for the Study of Surfaces and Interfaces of Solid Materials (LESIMS),
University Ferhat Abbas of Setif 1, Setif 19000, Algeria

^{||}Department of Electronic, Faculty of Technology, University of Mohamed Boudiaf,
M'sila 28000, Algeria

^{**}Department of Physics, College of Science, Taif University,
P. O. Box 11099, Taif 21944, Saudi Arabia
^{††}fatmimessaoud@yahoo.fr

Received 1 April 2023

Revised 19 May 2023

Accepted 11 June 2023

Published 14 August 2023

Structural, elastic, mechanical and electronic properties of pure and zinc-doped SrTiO₃ at the concentration in the range (1–10%) are studied by first-principles calculations. The structural parameters of synthesized compounds agree well with the standard data depicting the growth of stable compounds. A slight obvious increase in the lattice constant of 3.9245 Å is observed in Zn-doped SrTiO₃ due to the deviation of the atomic radii of Zn and Ti. Elastic constants and mechanical parameters of SrTiO₃ are closer to their available theoretical and experimental data. The investigated compounds exhibit brittle behavior for all Zn ratios. The doping zinc concentration reduces the indirect band gap value. The doping concentration 2%, gives a band gap value closer to the experimental one. The band gap of pure SrTiO₃ is 1.827 eV and after doping with Zn for concentration from 1% to 10%, the optimized values are 1.970, 1.886, 1.802, 1.718, 1.635, 1.552, 1.470, 1.389, 1.310, 1.231 and 1.154 eV.

Keywords: SrTiO₃; CASTEP; DFT; doping; elastic properties; electronic properties.

^{††} Corresponding author.

1. Introduction

The improvement of the conductivity and the photocatalytic capacity is obtained by introducing certain metallic elements such as Zn into the pure SrTiO_3 . The disadvantage of the photocatalytic system lies in their low use of visible light, the rapid recombination of charges and the low migration capacity of photo-generated electrons and holes. Therefore, noble and transition metals, nonmetals and metalloids are doped into the photocatalyst as co-catalyst to improve photodegradation performance.¹ Strontium perovskite titanate (SrTiO_3 or STO) shows high chemical stability, and abundance of constituent elements.² Eglitis and Kotomin give the results of Nb impurities substituting for Ti ions in SrTiO_3 using super cells containing up to 135 atoms.³ SrTiO_3 with a simple crystal structure is one of the most popular semiconductor used in photovoltaic applications and its mechanical properties are more sensitive to Sr-site cation.⁴ The determining factors in the ferroelectricity of SrTiO_3 are the decent ring, the geometric size and the electronic configuration of the Sr atoms. From the literature, we distinguish the transition from the parent cubic structure to the tetragonal one or from the rhombohedra phase to the orthorhombic or monoclinic structure.⁵ The calculated optical band gap of the cubic phase of SrTiO_3 is 3.57 eV and in very good agreement with experimental data.⁶ SrTiO_3 perovskite material exists in three phases depending on temperature; the orthorhombic phase exists below 100 K, the tetragonal structure in the range 100–300 K and the cubic one above 300 K, which is the most stable. Concerning the work carried out by other researchers, Ghebouli *et al.* studied some properties of SrMO_3 ($M = \text{Ti}$ and Sn) in their standard forms.⁷ The elastic constants of SrTiO_3 obtained from a polynomial fit to the energy–strain relation were calculated by both LDA and GGA approaches.⁸ SrTiO_3 has simple cubic perovskite structure at high temperature and goes through an anti-ferrodistortive AFD transition at 105 K to a tetragonal phase.⁹ The elastic characteristics of materials give the valuable data about the bonding property between adjacent atomic planes, bonding anisotropic, stiffness and structural stability of the material.¹⁰ The crystal anisotropy is related to the modulus of elasticity, has significance in the fields of engineering and material sciences and occurs when the relationship between stress and strain depends on its orientation.¹¹ Benrekia Ahmed Redha *et al.* presented a study on structural, electronic, vibrational and optical properties of para-electric SrTiO_3 .¹² Gulden Selik and Suleyman Cabuk reported electronic and optical properties of $\text{Sr}(\text{Ti}, \text{Zr})\text{O}_3$ crystals in the cubic ($\text{Pm}-3\text{m}$) and tetragonal ($\text{I}4/\text{mcm}$) phase using the local density approximation.¹³ The current work emphasizes investigating the structural, mechanical and electronic properties of Zn-doped SrTiO_3 . The Zn concentration is varied to optimize the appropriate content in SrTiO_3 matrix for potential applications. The doping of SrTiO_3 by zinc atoms allows this new material to have a suitable band gap and absorption factor in order to use it as an absorber in photovoltaic cells. Zinc impurities favor replacing Ti ion instead of Sr and O-ion in SrTiO_3 . In the doped sample, Zn atoms in proportions that vary in the range 1–10% replace the Ti atoms.

Density functional theory with generalized gradient approximation (GGA-PBE) was employed to achieve the stability of Zn-doped SrTiO_3 through elastic constant and tolerance factor. We attempted to synthesize $\text{SrZn}_x\text{Ti}_{(1-x)}\text{O}_3$ nanopowder experimentally. The doping of SrTiO_3 by Zn induces variations in the studied properties and opens up new prospects for potential applications of this material in the optoelectronic field. The structural, elastic, mechanical, electronic and optical properties were investigated.

2. Computation Details

First-principles calculations were performed in the DFT framework with GGA-PBE approximations using the CASTEP code.¹⁴ The ultra-soft-pseudopotential method and the GGA-PBE approximation functional¹⁵ describe the exchange-correlation effect. The best convergence of the computed structures and energies requires the use of Monkhorst–Pack points of $6 \times 6 \times 6$ grid and cut-off energy of 800 eV.¹⁶ The calculation of the optical quantities requires the use of dense mesh of uniformly distributed $20 \times 20 \times 20$ k -points. The minimization technique of Broyden–Fletcher–Goldfarb–Shanno¹⁷ determines the structural parameters, which provides a fast way to find the lowest energy structure. The tolerance for geometry optimization was performed with affinity resolution of the set as the difference of total energy 10^{-5} eV/atom, maximum ionic Hellmann–Feynman force 3×10^{-2} eV/Å and maximum stress 2×10^{-2} eV/Å³. The approach adopted in this study facilitates the calculation of the forces and stresses involved, controls the convergence of every computational parameter and neglects the effect of nucleus electrons.

3. Results and Discussions

3.1. Structural parameters

The structure of pure and Zn-doped SrTiO_3 material was optimized using CASTEP and GGA-PBE core assembly. The electronic configuration of Sr, Ti, Zn and O is $4s^24p^65s^2$, $3s^23p^63d^24s^2$, $3d^{10}4s^2$ and $2s^22p^4$. Figure 1 shows the crystal structure of standard SrTiO_3 . The optimized lattice constant, bulk modulus and its pressure derivative of pure and Zn-doped SrTiO_3 are reported in Table 1. The reliability of the mentioned results is evident from the correlation between theoretical^{18–20} and experimental²¹ data. It is observed that the optimized lattice constant, which corresponds to a Zn content of 1%, is 3.924 Å. This result is consistent with the experimental value of 3.905 Å cited in the literature.²¹ However, our calculations report a lattice constant of 3.9849 Å for Zn content of 9%.

It is noted that SrTiO_3 doped by Nb with a percentage of 1%, 2%, 3%, 5% and 8% shows a lattice constant of 3.9078, 3.9088, 3.9066, 3.905 and 3.9063 Å.^{22,23} The value of the lattice constant of SrTiO_3 doped by Nb with a percentage of 25% and 50% is about 3.969 and 4 Å,²⁴ which is closer to the experimental value of 3.980 and 4.002 Å.²⁵ A slight obvious increase in the lattice constant of 3.9245 Å is observed in

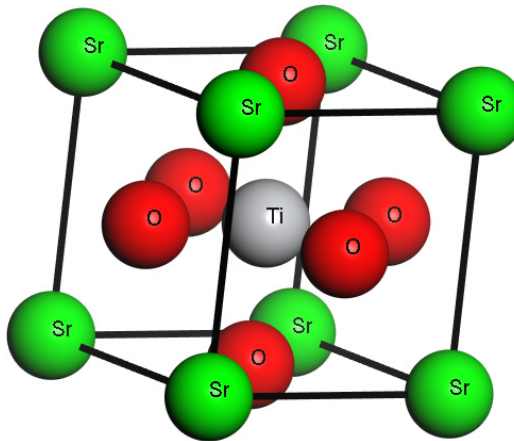
Fig. 1. (Color online) Crystal structures of SrTiO_3 compound.

Table 1. Lattice constant, volume, bulk modulus and its pressure derivative for standard and Zn-doped SrTiO_3 with available theoretical and experimental published data.

Compound	a_0 (\AA)	V (\AA^3)	B_0 (GPa)	B'_0
SrTiO_3	3.917	60.13	173.02	4.33
	3.919 ¹⁸			4.712 ¹⁹
	3.904 ¹⁹		190.67 ¹⁹	
	3.940 ²⁰			
	3.905 ²¹ exp.			
$\text{SrZn}_{0.02}\text{Ti}_{0.98}\text{O}_3$	3.9315	60.7701	168.61	4.36
$\text{SrZn}_{0.03}\text{Ti}_{0.97}\text{O}_3$	3.9387	61.1039	166.69	4.37
$\text{SrZn}_{0.04}\text{Ti}_{0.96}\text{O}_3$	3.9459	61.4390	164.45	4.38
$\text{SrZn}_{0.05}\text{Ti}_{0.95}\text{O}_3$	3.9534	61.7890	162.32	4.40
$\text{SrZn}_{0.06}\text{Ti}_{0.94}\text{O}_3$	3.9610	62.1492	159.38	4.42
$\text{SrZn}_{0.07}\text{Ti}_{0.93}\text{O}_3$	3.9688	62.5164	157.07	4.44
$\text{SrZn}_{0.08}\text{Ti}_{0.92}\text{O}_3$	3.9768	62.8942	154.37	4.46
$\text{SrZn}_{0.09}\text{Ti}_{0.91}\text{O}_3$	3.9849	63.28	151.41	4.48
$\text{SrZn}_{0.1}\text{Ti}_{0.90}\text{O}_3$	3.9931	63.67	149.55	4.50

Zn-doped SrTiO_3 due to the deviation of the atomic radii of Zn and Ti. The total energy versus volume was plotted for SrTiO_3 in the standard state and by doping it with Zn (Zn = 2%, 5% and 10%), as shown in Fig. 2. Optimization of SrTiO_3 and $\text{SrTi}_{(1-x)}\text{Zn}_x\text{O}_3$ structures for various Zn contents was achieved by fitting Murnaghan's equation of state.²⁶ It is noted that the introduction of a percentage of Zn makes the structure less stable.

The lattice constant, volume and bulk modulus as a function of zinc content x for $\text{SrZn}_x\text{Ti}_{1-x}\text{O}_3$ alloys are shown in Fig. 3. The volume was observed to decrease as Zn content increases in SrTiO_3 . The lattice constant (bulk modulus) increases (decreases) with increasing Zn content. The fit of our data regarding the lattice

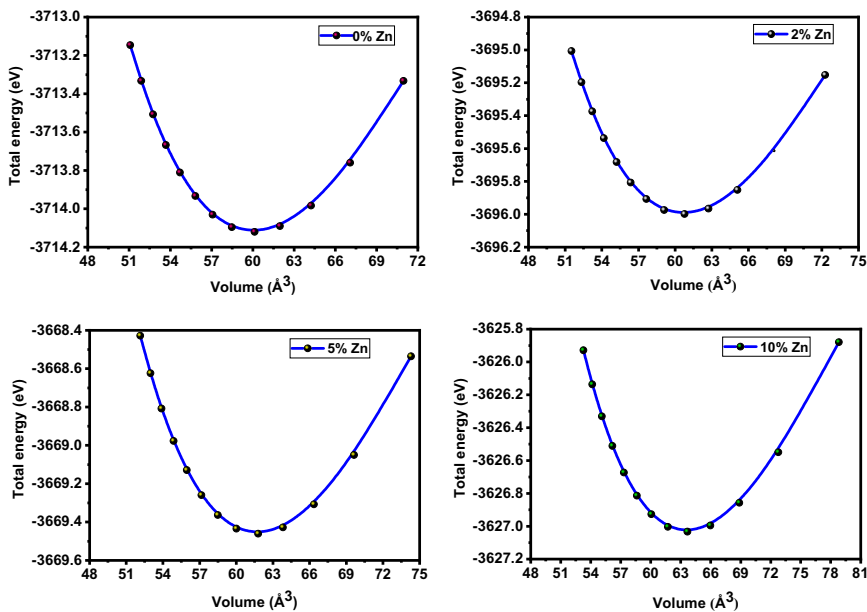


Fig. 2. (Color online) Total energy versus volume for standard and Zn-doped SrTiO_3 ($\text{Zn} = 2\%, 5\%$ and 10%).

constant, the volume and bulk modulus obeys these polynomial expressions:

$$a_0(x) = 3.9176 + 0.0067x + 7.9 \times 10^{-5}x^2, \quad (1)$$

$$V(x) = 60.1287 + 0.3105x + 0.0043x^2, \quad (2)$$

$$B_0(x) = 172.87 - 1.99x - 0.03x^2. \quad (3)$$

The dynamic stability of SrTiO_3 is studied by visualizing the phonon dispersion curves and their total densities of state, as shown in Fig. 4. SrTiO_3 is dynamically stable due to the non-presence of imaginary phonon frequencies. We will not be able to visualize the spectrum of phonons for a concentration of Nb, because it requires a sophisticated calculation tool that we lack.

3.2. Elastic constants and mechanical characteristics

The elastic constants describe the response to applied macroscopic stress and relate the mechanical parameters to the elasticity, stability and stiffness.²⁷ Understanding the mechanical properties of a material due to the response of external forces requires the use of elastic constants. Mechanical properties include Young's modulus (E), elastic hardness coefficients (C_{ij}), bulk modulus (B), shears modulus (G), Poisson's ratio and anisotropy (A). The stability of the structure and the heterogeneous bond between neighboring atoms are described by the elastic constants of the material. Shear and Young moduli describe the stiffness of the bond and the resistance to deformation and fracture. Elastic constants are related to basic phenomena such as

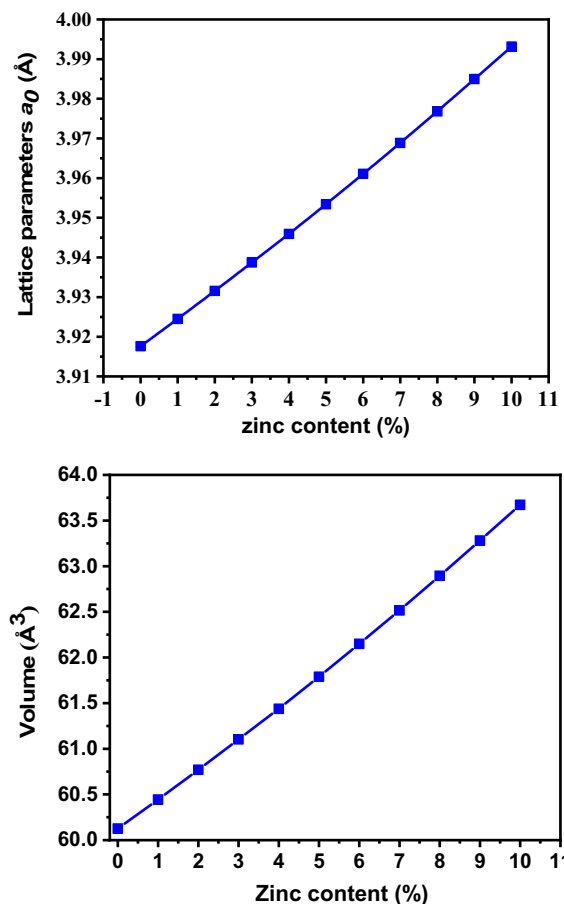


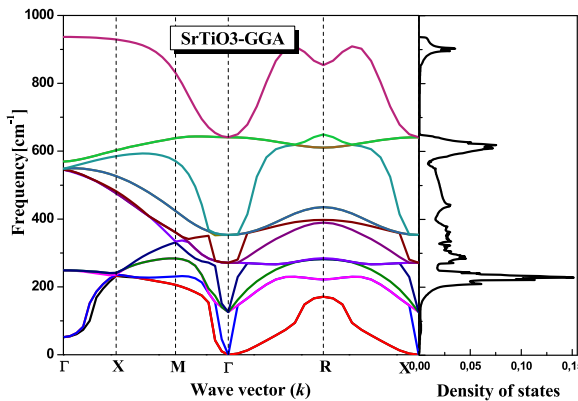
Fig. 3. (Color online) Volume and lattice constant versus zinc content x in $\text{SrZn}_x\text{Ti}_{1-x}\text{O}_3$.

brittleness, ductility, hardness and mechanical stability of the material. Elastic constants provide information about the structure stability, bond behavior, anisotropy and cohesion of a material. C_{11} , C_{12} and C_{44} of SrTiO_3 cubic structure at zero pressure are enlisted in Table 2, which are consistent with their theoretical 350.46, 101.16 and 111.02 GPa¹⁹ and experimental^{4,28} values. Computed elastic moduli for pure and Zn-doped SrTiO_3 are positive and satisfy the following generalized conditions to ensure their elastic stability^{29,30}:

$$C_{11} + 2C_{12} > 0, \quad C_{44} > 0, \quad C_{11} - C_{12} > 0, \quad C_{12} \langle B/C_{11} \rangle > 0. \quad (4)$$

Note that C_{11} is larger and stiffer than C_{12} and C_{44} .

The bulk modulus represents the compressive strength of the material; therefore, SrTiO_3 shows perfect volume compressive strength. The bulk modulus, anisotropy factor, shear and Young's moduli, B/G and Poisson's ratios and Vickers hardness of undoped and Zn-doped SrTiO_3 are reported in Table 2. The Vickers hardness of

Fig. 4. (Color online) Phonon dispersion curves and density of states of SrTiO_3 .Table 2. Elastic constants, Shear and Young's moduli, B/G ratio, anisotropy factor, hardness and Poisson's ratio of $\text{SrZn}_x\text{Ti}_{(1-x)}\text{O}_3$.

	C_{11} (GPa)	C_{12} (GPa)	C_{44} (GPa)	G (GPa)	Y (GPa)	B/G	A	H (GPa)	σ
SrTiO_3	317.62	99.71	113.32	111.5	275	1.55	0.98	16.7	0.23
Exp. [24.4.25]	317	102.5	112	95.7	236.3	1.54	1.02		
$\text{SrZn}_{0.02}\text{Ti}_{0.98}\text{O}_3$	318.20	100.15	113.17	111.47	275.24	1.5525	1.03	16.70	0.23
$\text{SrZn}_{0.03}\text{Ti}_{0.97}\text{O}_3$	318.17	100.14	113.14	111.45	275.20	1.5526	1.03	16.70	0.23
$\text{SrZn}_{0.04}\text{Ti}_{0.96}\text{O}_3$	318.13	100.12	113.12	111.43	275.16	1.5527	1.03	16.70	0.23
$\text{SrZn}_{0.05}\text{Ti}_{0.95}\text{O}_3$	318.10	100.11	113.09	111.41	275.11	1.5528	1.03	16.69	0.23
$\text{SrZn}_{0.06}\text{Ti}_{0.94}\text{O}_3$	318.07	100.09	113.07	111.40	275.07	1.5629	1.03	16.69	0.23
$\text{SrZn}_{0.07}\text{Ti}_{0.93}\text{O}_3$	318.04	100.08	113.04	111.38	275.02	1.5530	1.03	16.69	0.23
$\text{SrZn}_{0.08}\text{Ti}_{0.92}\text{O}_3$	318.01	100.07	113.02	111.36	274.98	1.5530	1.03	16.69	0.23
$\text{SrZn}_{0.09}\text{Ti}_{0.91}\text{O}_3$	317.98	100.05	112.99	111.34	274.94	1.5531	1.03	16.68	0.23
$\text{SrZn}_{0.1}\text{Ti}_{0.90}\text{O}_3$	317.95	100.04	112.97	111.32	274.90	1.5532	1.03	16.68	0.23

$\text{SrZn}_x\text{Ti}_{(1-x)}\text{O}_3$ was estimated using the semi-empirical model $H = 0.0607 \times Y$.³¹ The mechanical characteristics of the $\text{SrZn}_x\text{Ti}_{(1-x)}\text{O}_3$ materials behavior were described under Zn content effect.^{32,33} Figure 5 shows the dependence of elastic constants on zinc content for $\text{SrZn}_x\text{Ti}_{1-x}\text{O}_3$ alloys according to GGA-PBE approximation. It is noted that all these parameters decrease almost monotonously with the addition of zinc content. The bulk and shear moduli of Voigt and Reus limit for a cubic crystal are given as

$$B = (B_R + B_v)/2, \quad (5)$$

$$G = (G_v + G_R)/2. \quad (6)$$

Young's modulus, Poisson's ratio and anisotropic factor can be obtained by

$$E = 9GB/(3B + G), \quad (7)$$

$$\sigma = (3B - 2G)/(3B + G), \quad (8)$$

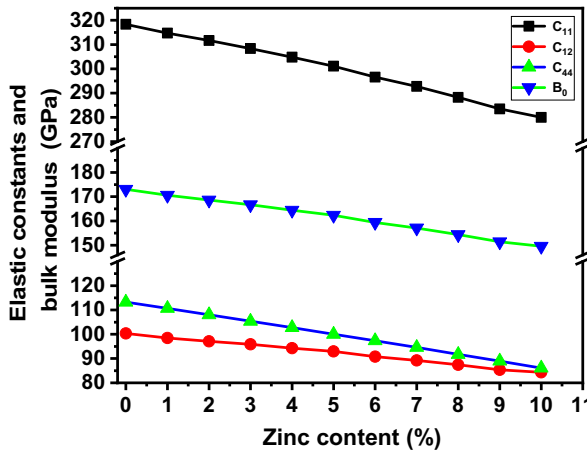


Fig. 5. (Color online) Elastic constants and bulk modulus versus zinc content x for $\text{SrZn}_x\text{Ti}_{1-x}\text{O}_3$ alloys.

$$A = 2C_{44}/(C_{11} - C_{12}). \quad (9)$$

B/G ratio describes the ductility and brittleness of material, if this ratio is greater than 1.75, the material is ductile, otherwise it exhibits fragile nature. The B/G ratio for pure and Zn-doped SrTiO_3 is less than 1.75 indicating its brittleness.

Figure 6 depicts the nonlinear behavior of B/G ratio as a function of Zn concentration. Young's modulus and Shear modulus exhibit a decreasing trend for the strain with increasing concentration of zinc as shown in Fig. 7.

The quoted values are in good agreement with those reported in the literature¹⁹ and experiments.³⁴ The Poisson ratio determines the stability of the material and the nature of bonding forces. The poisson ratio is 0.23, indicating the significant ionic contribution

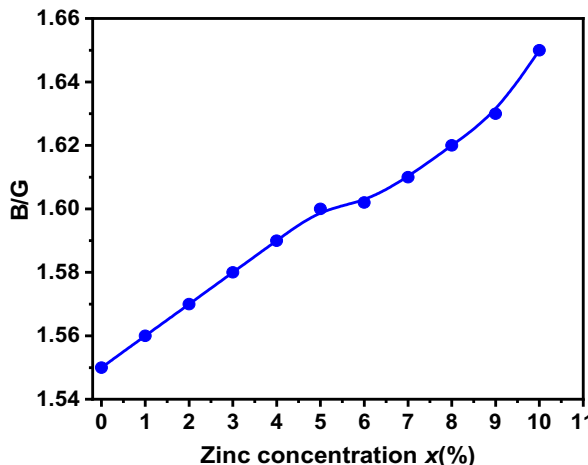


Fig. 6. (Color online) B/G as a function of zinc content x for $\text{SrZn}_x\text{Ti}_{1-x}\text{O}_3$ alloys.

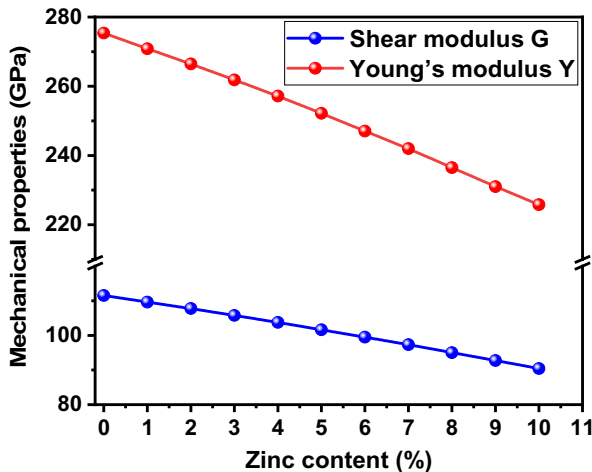


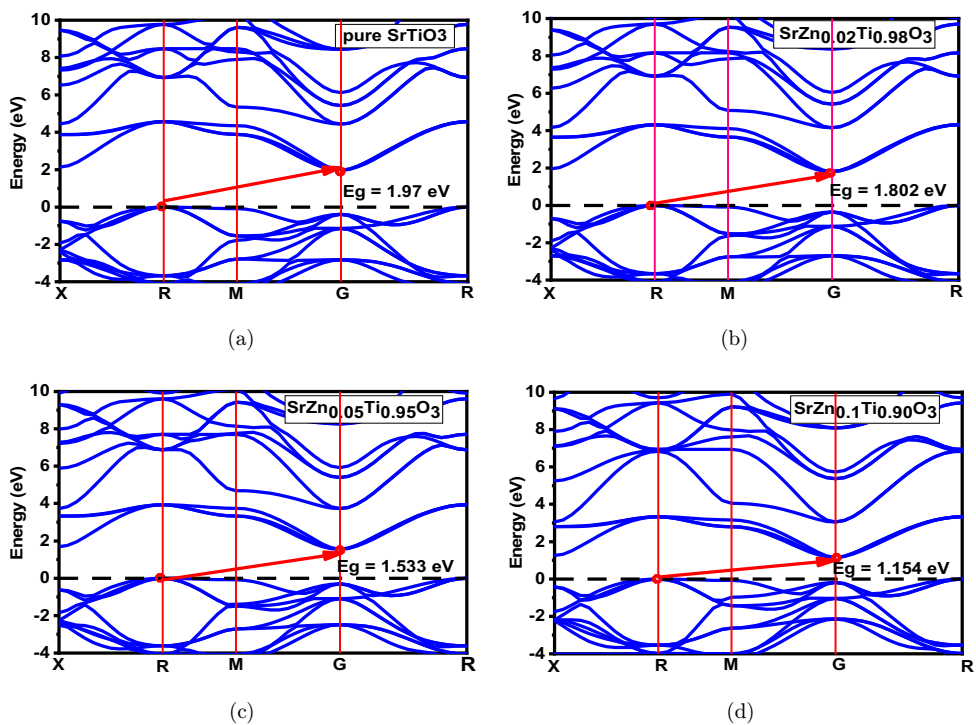
Fig. 7. (Color online) Shear and Young's Modulus as a function of zinc content x for $\text{SrZn}_x\text{Ti}_{1-x}\text{O}_3$ alloys.

towards intra-atomic bonding. SrTiO_3 is isotropic because the elastic anisotropy value is close to unity. The resistivity of this material to the deformation was studied using mechanical parameters.³⁵ Cauchy pressure ($C_p = C_{12} - C_{44} < 0$) shows that $\text{SrZn}_x\text{Ti}_{(1-x)}\text{O}_3$ is covalent in nature.³⁶ The values of Young's modulus compared to the large bulk modulus indicate that this material is more difficult to crush.

3.3. Electronic properties

Electronic properties, in particular the energy gap, help in understanding the nature of bonds, electronic conductivity, optical behavior and stability. It is noted that the energy gap influences the optical characteristics responsible for the photocatalytic properties of the material. The determination of the band structure provides information on the nature of the compound, whether it is conductor, semi-conductor or insulator. The band structures as a function of zinc content x for $\text{SrZn}_x\text{Ti}_{1-x}\text{O}_3$ ($x = 0\%, 2\%, 5\%$ and 10%) alloys are shown in Fig. 8. The energy band structure for standard SrTiO_3 demonstrated a valence band in the range from -5 eV to 0 eV and a conduction band in the range from 2.20 eV to 5 eV . It is noticed that the observed energy gap is 1.97 eV , as shown in Fig. 8(a). This value is comparable to those reported by experiment, which are 1.92 eV ³⁷ and 1.90 eV ³⁸ and other theoretical values.^{6,39}

The maximum valence band is located at the Fermi level, so all the studied compounds are semiconducting in nature, with indirect $R \rightarrow \Gamma$ band gap. The separation between conduction and valence bands is due to the large number of electrons in their corresponding bands and thus in the occupancy states close to the Fermi level.³⁹ All calculated band gap values of Zn-doped SrTiO_3 at 0 GPa are shown in Table 3.

Fig. 8. (Color online) Calculated band structure as a function of zinc content for $\text{SrZn}_x\text{Ti}_{1-x}\text{O}_3$ alloys.Table 3. Calculated band gap value of Zn-doped SrTiO_3 at 0 GPa.

x (%) Zn content	E_g (eV) This work	E_g (eV) Other	E_g (eV) Experiment
0	1.97 55	1.84 ³⁹ 1.99 ⁶	1.92 ³⁷ 1.90 ³⁸
2	1.802	—	—
5	1.533	—	—
10	1.154	—	—

Figure 9 shows the variation in band gap energy as a function of Zn concentration. Note that there is a linear decrease in the band gap when Zn content is enhanced. The reduced band gap energy of the Zn-doped SrTiO_3 compounds leads to an argument that studied compounds can offer upgraded optical properties. The reduction of the energy gap with the increase of the doping by Zn content allows the studied compound to improve the optical properties. By doping SrTiO_3 with Zn content varying in the range 1–10%, the energy gap is located in the interval 1.802–1.154 eV. The fit of our data regarding the variation of E_g as a function of Zn content

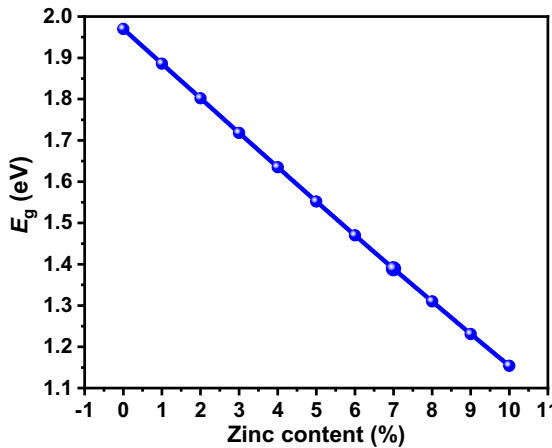


Fig. 9. (Color online) Band gap as a function of zinc content for $\text{SrZn}_x\text{Ti}_{1-x}\text{O}_3$ alloys.

x obeys the second-order polynomial expressions:

$$E_g(x) = 1.97113 - 0.08581x + 3.99767 \times 10^{-4}x^2. \quad (10)$$

The character of the band structure and the trend of the energy gap versus Zn content are reasonable and reliable. The calculation of the band structure intuitively describes the effect of doping on the energy gap. For the 5%, 10% and 20% S-doped SrTiO_3 the band gap energy is 2.87, 2.73 and 3 eV.⁴⁰ The value of the energy gap of $\text{SrTi}_{0.875}\text{Nb}_{0.125}\text{O}_3$ is about 1.85 eV, which is small with respect to the experimental value of about 3.2 eV.²⁴ The growth of Al concentrations of 10% and 20%-doped SrTiO_3 films on Si(100) substrate indicates that the band gap is increased by 0.3 eV over undoped SrTiO_3 .⁴¹ The Ag-doping on SrTiO_3 reduces the band gap by 0.15 eV.⁴² The transition metal dopant has no effect on STO band gap, except for Pd and Pt that are able to reduce the STO band gap, while doping S and Se significantly reduces STO's band gap.⁴³ The resulting band gap values 3.09, 3.12 and 3.17 eV are related to the Nb-doped SrTiO_3 with 20%, 30% and 10%.⁴⁴ The total and partial densities of states analyze the physical properties of the material and give the detailed electronic contribution of the states of the elements Sr, Ti, Zn and O, which constitute the studied element. The TDOS and PDOS for standard and Zn (10%)-doped SrTiO_3 computed using GGA-PBE approximation are illustrated in Fig. 10. Note that the lower valence bands for SrTiO_3 and $\text{SrZn}_{(0.1)}\text{Ti}_{(0.9)}$ are located in the range -20 eV to -10 eV energy levels. These bands consist of Sr-*p* and Sr-*s* states for SrTiO_3 and Sr-*p*, O-*p*, Zn-*s* and Zn-*p* for $\text{SrZn}_{(0.1)}\text{Ti}_{(0.9)}$. The high valence bands lie from about -5 eV to the Fermi level and consist mainly of Sr-*p*, Sr-*d* and O-*p* states for SrTiO_3 , and Ti-*p*, Ti-*d*, O-*p* and Zn-*d* and Zn-*p* for $\text{SrZn}_{(0.1)}\text{Ti}_{(0.9)}$. However, near the Fermi level, the contributions of Sr-*p*, Sr-*d* and O-*p* states for SrTiO_3 and Ti-*p*, Ti-*d* and O-*p* states for $\text{SrZn}_{(0.1)}\text{Ti}_{(0.9)}$ predominate. The increase in Zn content leads to the mixing of Zn-*p* and Zn-*d* with O-*p*, and therefore the band gap is reduced.

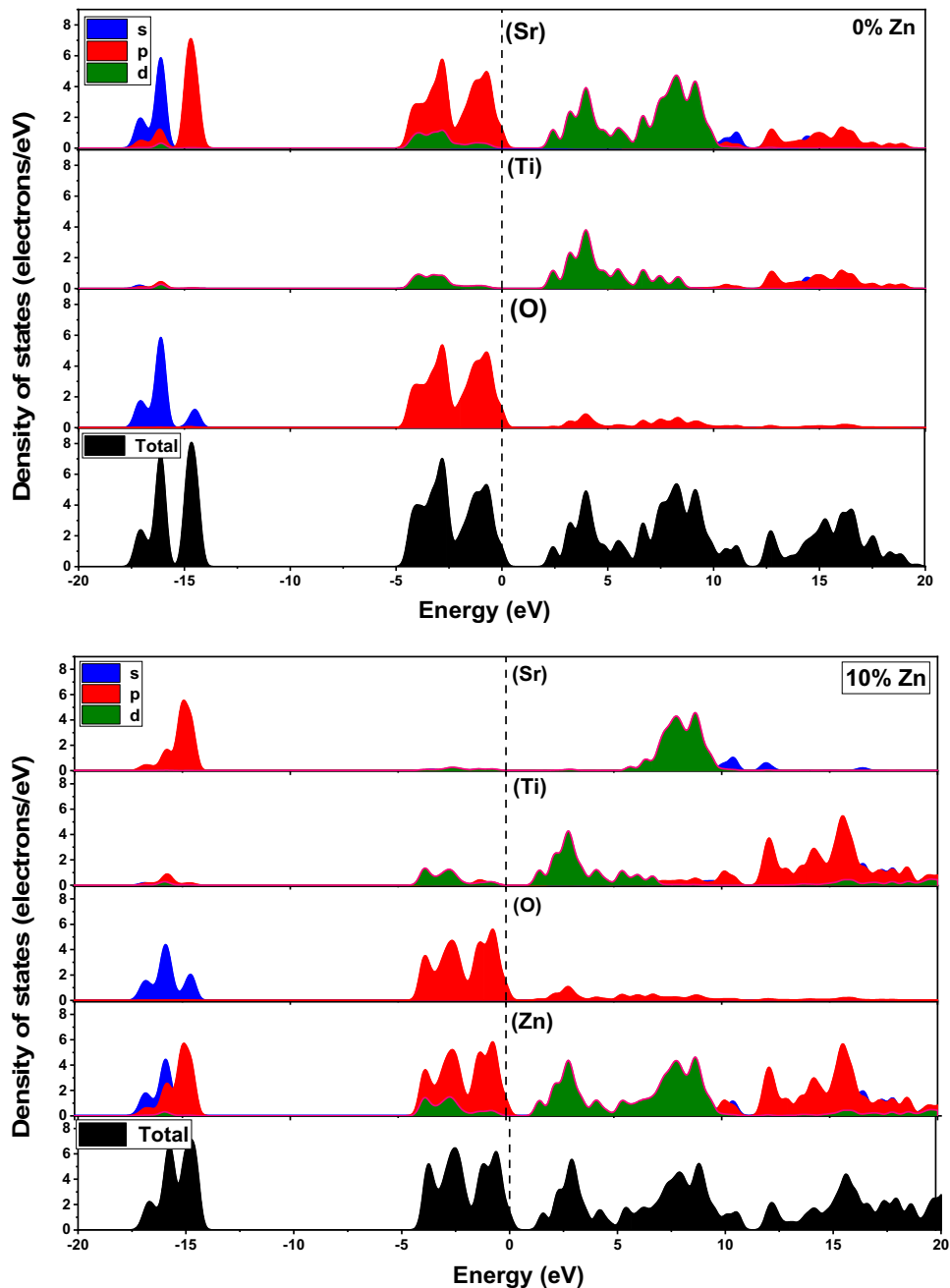


Fig. 10. (Color online) TDOS and PDOS for standard and Zn (10%)-doped SrTiO_3 using GGA-PBE approximation.

4. Conclusion

Structural, elastic, mechanical and electronic properties of pure and Zn-doped SrTiO₃ compounds have been investigated using first-principles calculation via the CASTEP code. The investigated compounds exhibit an isotropic cubic structure with brittle nature. The Zn-doped SrTiO₃ (10%) is observed to be the most stable compound with narrow band gap energy. The substitution of Ti atoms by those of Zn improves the photocatalytic activity of SrTiO₃ compound. The band structure of SrZn_xTi_{1-x}O₃ alloys exhibits an indirect $R \rightarrow \Gamma$ band gap. The partial and total DOS analysis shows that the conduction band is mainly composed of Zn and Ti-*d* with a mixture of Sr-*s* and Sr-*d* states of SrTiO₃, while O-*p* is mainly dominated by the valence band states. The increase in Zn content leads to the mixing of Zn-*p* and Zn-*d* with O-*p*, and therefore the band gap is reduced. The characterizations of pure and Zn-doped SrTiO₃ materials suggest that these materials have a significant potential to be used in photocatalytic devices. The doping of SrTiO₃ compound by Zn atoms shifts the top of the valence band towards the Fermi level.

Acknowledgments

The researchers would like to acknowledge the Deanship of Scientific Research, Taif University for funding this work.

References

1. W. S. Koe, J. W. Lee, W. Ch. Chong, Y. L. Pang and L. Ch. Sim, *Environ. Sci. Pollut. Res.* **27** (2020) 2522, doi: 10.1007/s11356-019-07193-5.
2. P. Reunchan, S. Ouyang, N. Umezawa, H. Xu, Y. Zhang and J. Ye, *J. Mater. Chem. A* **1** (2013) 4121, doi: 10.1039/C2TA00450J.
3. R. I. Eglitis and E. A. Kotomin, *Phys. B: Condens. Matter* **405** (2010) 3164, doi: 10.1016/j.physb.2010.04.033.
4. N. Pandech, K. Sarasamak and S. Limpijumnong, *J. Appl. Phys.* **117** (2015) 174108, doi: 10.1063/1.4919837.
5. M. A. Carpenter, *Am. Mineral* **92**(2–3) (2007) 309, doi: 10.2138/am.2007.2295.
6. S. Piskunov, E. Heifets, R. I. Eglitis and G. Borstel, *Comput. Mater. Sci.* **29** (2004) 165, doi: 10.1016/j.commatsci.2003.08.036.
7. B. Ghebouli, M. A. Ghebouli, T. Chihi, M. Fatmi, S. Boucetta and M. Reffas, *Solid State Commun.* **149**(47–48) (2009) 2244, doi: 10.1016/j.ssc.2009.09.001.
8. N. Pandech, K. Sarasamak and S. Limpijumnong, *J. Chin. Chem. Soc.* **63** (2016) 521, doi: 10.1002/jccs.201500377.
9. M. E. Lines and A. M. Glass, *Principles and Applications of Ferroelectrics and Related Materials* (Clarendon Press, Oxford, 1977).
10. J. S. Edrees, M. M. Shuker and M. M. Obeid, *Comput. Condens. Matter* **14** (2018) 20.
11. C. M. Kube, *AIP Adv.* **6** (2016) 095209, doi: 10.1063/1.4962996.
12. A. R. Benrechia, N. Benkhetto, A. Nassour, M. Dris, M. Sahnoun and S. Lebègue, *Phys. B Condens. Matter* **407**(13) (2012) 2632, doi: 10.1016/j.physb.2012.04.013.
13. G. Celik and S. Cabuk, *Cent. Eur. J. Phys.* **11**(3) (2013) 387. https://DOI: 10.2478/s11534-013-0176-6.

14. M. A. Ghebouli, B. Ghebouli, L. Krache, S. Alomairy, M. Fatmi, T. Chihi and M. Reffas, *Bull. Mater. Sci.* **45**(3) (2022) 124.
15. J. P. Perdew, K. Burke and M. Ernzerhof, *Phys. Rev. Lett.* **77** (1996) 3865, doi: 10.1103/PhysRevLett.77.3865.
16. H. J. Monkhorst and J. D. Pack, *Phys. Rev. B* **13** (1976) 5188, doi: 10.1103/PhysRevB.13.5188.
17. T. H. Fischer and J. Almlöf, *J. Phys. Chem.* **96** (1992) 9768, doi: 10.1021/j100203a036.
18. Y. Naceur, H. Bourbaba, M. A. Ghebouli, L. Krache, B. Ghebouli, T. Chihi and S. Alomairy, *Sci. Rep.* **12**(1) (2022) 1.
19. K. Bouferrache, M. A. Ghebouli, B. Ghebouli, M. Fatmi, S. Alomairy and T. Chihi, *Chin. J. Phys.* **81** (2023) 303.
20. S. A. Saoucha, I. Bouchama, S. Alomairy, M. A. Ghebouli, B. Ghebouli and M. Fatmi, *Solid State Commun.* **354** (2022) 114897.
21. K. van Benthem, C. Elsasser and R. H. French, *J. Appl. Phys.* **90**(12) (2001) 6156.
22. J. Karczewski, B. Riegel, M. Gazda, P. Jasinski and B. Kusz, *J. Electroceram.* **24** (2010) 326, doi: 10.1007/s10832-009-9578-7.
23. T. Zhao, H. Lu, F. Chen, S. Dai, G. Yang and Z. Chen, *J. Cryst. Growth* **212**(3–4) (2000) 451.
24. X. G. Guo, X. S. Chen, Y. L. Sun, L. Z. Sun, X. H. Zhou and W. Lu, *Phys. Lett. A* **317** (2003) 501.
25. T. Tomio, H. Miki, H. Tabata, T. Kawai and S. Kawai, *J. Appl. Phys.* **76** (1994) 5886.
26. F. D. Murnaghan, *Proc. Natl. Acad. Sci. USA* **30** (1944) 5390.
27. M. Zafar, M. Shakil, S. Ahmed, M. Hashmi, M. A. Choudhary and Naeem-ur-Rehman, *Sol. Energy* **158** (2017) 63.
28. D. Berlincourt and H. Jaffe, *Phys. Rev.* **111** (1958) 143.
29. H. B. Huntington, *Solid State Phys.* (1958) 213, doi: 10.1016/s0081-1947(08)60553-6.
30. M. Shakil, H. Arshad, M. Zafar, M. Rizwan, S. S. A. Gillani and S. Ahmed, *Mol. Phys.* (2020) 1789770, doi: 10.1080/00268976.2020.1789770.
31. X. Jiang, J. Zhao and X. Jiang, *Comput. Mater. Sci.* **50** (2011) 2287.
32. M. Shakil, A. Akram, I. Zeba, R. Ahmad, S. Gillani and M. Gadhi, *Mater. Res. Express* **7**(2) (2020) 025513, doi: 10.1088/2053-1591/ab727d.
33. M. Zafar, M. Kashif, M. Rizwan, A. Zia, S. Ahmad, A. Akram, C. C. Bao and M. Shakil, *Optik* **182** (2019) 1176.
34. R. O. Bell and G. Ruprecht, *Phys. Rev.* **129** (1963) 90.
35. R. S. Sunmonu, O. Y. Fadimu and O. I. Sonde, *Int. J. Mod. Phys. B* (2023).
36. A. Afafq, A. Bakar, S. Anwar, W. Anwar and Fazal-e-Aleem, *Int. J. Mod. Phys. B* **32** (2018) 1850362, doi: 10.1142/S0217979218503629.
37. J. Robertson, K. Xiong and S. J. Clark, *Thin Solid Films* **496** (2006) 1.
38. E. Mete, R. Shaltraf and S. Ellialtioglu, *Phys. Rev. B* **68** (2003) 035119.
39. J. Yun, T. Yin and Z. Zhang, *Adv. Mater. Res.* **750–752** (2013) 1199, doi: 10.4028/www.scientific.net/AMR.750-752.1199.
40. H. K. Le, K. O. Pham, T. T. Tran and M. V. Le, *Sci. Technol. Dev.* **19**(K6) (2016) 176.
41. A. B. Posadas, C. Lin, A. A. Demkov and S. Zollner, *Appl. Phys. Lett.* **103** (2013) 142906, doi: 10.1063/1.4824023.
42. S. A. Azevedo, J. A. S. Laranjeira, J. L. P. Ururi and E. Longo, *Comput. Mater. Sci.* **214**(4) (2022) 111693, doi: 10.1016/j.commatsci.2022.111693.
43. Y. S. Hou, S. Ardo and R. Q. Wu, *Phys. Rev. Mater.* **5** (2021) 065801.
44. M. A. K. Yousaf Shah, S. Rauf, B. Zhu, N. Mushtaq, M. Yousaf, P. D. Lund, C. Xia and M. I. Asghar, *ACS Appl. Energy Mater.* **4**(1) (2021) 365.